ChemComm

Distinguishing Between Bulk and Edge Hydroxyl Vibrational Properties of 2:1 Phyllosilicates via Deuteration

Journal:	*ChemComm*
Manuscript ID	CC-COM-01-2019-000164.R1
Article Type:	Communication

Journal Name

ARTICLE

Distinguishing Between Bulk and Edge Hydroxyl Vibrational Properties of 2:1 Phyllosilicates via Deuteration

Jacob A. Harvey,[a*] Cliff T. Johnston,[b] Louise J. Criscenti,[a] Jeffery A. Greathouse[a]

Received 00th January 20xx,
Accepted 00th January 20xx

DOI: 10.1039/x0xx00000x

www.rsc.org/

Observation of vibrational properties of phyllosilcate edges via a combined molecular modeling and experimental approach was performed. Deuterium exchange was utilized to isolate edge vibrational modes from their internal counterparts. The appearance of a specific peak within the broader D_2O band indicates the presence of deuteration on the edge surface, and this peak is confirmed with the simulated spectra. These results are the first to unambiguously identify spectroscopic features of phyllosilcate edge sites.

Due to their large surface areas and highly structured interlayer galleries, phyllosilicate minerals, play a major role in a number of processes including underground sequestration and the attenuation of contaminants in the subsurface.[1] Developing a molecular level understanding of the associated adsorption and transport processes is paramount to utilizing these critical minerals in subsurface technical applications. While numerous experimental techniques exist for probing the atomic structure of layered minerals,[2] their results are often difficult to interpret in the absence of molecular modeling approaches. Classical molecular dynamics (MD) simulations based on approximate force field (FF) expressions for interatomic interactions have proven to be quite successful at predicting various clay properties including swelling and hydration,[3] ion exchange,[4] and adsorption of organic molecules.[5]

Basal surfaces comprise the majority of accessible surface area of phyllosilicates; upwards of 80%,[6] but the siloxane sheets that distinguish these surfaces are chemically inert. Smectite clay minerals such as montmorillonite bear a permanent negative surface charge due to isomorphic cation substitution within the lattice structure, resulting in strong adsorption of extra framework cations via pH-*independent* ion exchange. Yet these minerals are known to exhibit pH-*dependent* adsorption behavior at amphoteric edge sites.[7] FF modeling can now provide important molecular-level details of ion adsorption processes at these sites, particularly for environmentally relevant metal cations such as transition metals[8] and radionuclides.[9]

The tetrahedral (Si) and octahedral (Al) coordination environment of layer cations in the bulk is disrupted at phyllosilicate edges. These undercoordinated sites are thought to be terminated by hydroxyl groups formed by water dissociation during mineral growth or dissolution processes. Unfortunately, an unambiguous identification of the local coordination environment of these edge sites by diffraction or spectroscopic methods remains elusive, particularly since these edges comprise such a small fraction of total surface area. An additional and important complication in the spectroscopic characterization of phyllosilicate edge sites is that the bulk crystal structures also contain hydroxyl groups within the first shell of octahedrally coordinated layer cations (e.g., Al, Mg). Finally, many phyllosilicates such as the smectites and kaolinite are strongly hydrophilic, so the presence of adsorbed water further complicates the spectroscopic signature of hydroxyl-containing functional groups.

Here we employ a novel method of obtaining the infrared (IR) spectrum of phyllosilicate edge sites by exposing a dried mineral sample to deuterated water (D_2O). D_2O in contact with reactive edge sites gives rise to IR peaks due to both adsorbed D_2O and edge OD groups, which are well shifted from their proton counterparts. Such a method has been used previously to examine hydroxyl frequencies of iron (oxy)hydroxides,[10] and water structure in smectites.[11] For this work we use the neutral endmember of the smectite series, pyrophyllite ($Al_2Si_4O_{10}(OH)_2$) (Fig. 1). Pyrophyllite is a dioctahedral non-swelling mineral whose basal siloxane surfaces are generally considered to be hydrophobic,[12] similar to its trioctahedral equivalent, talc.[13] However, water readily

[a] *Geochemistry Department, Sandia National Laboratories, Albuquerque, New Mexico 87125, United States. Email: jharve@sandia.gov*
[b] *Crop, Soil and Environmental Sciences, Purdue University, West Lafayette, Indiana 47907, United States.*

†Electronic Supplementary Information (ESI) available: Full computational and experimental methods, time evolution of simulated pressure for bulk pyrophyllite, tests and validation of simulated IR spectra calculations, successive drying experimental spectra, deuterated edge bending region of IR spectra, MD IR spectra for the 110 face, and DFT vibrational calculations. See DOI: 10.1039/x0xx00000x

adsorbs at the more hydrophilic edge sites, and the adsorbed structure can be interrogated with IR spectroscopy. We compare the experimental spectra with calculated IR spectra from molecular simulations at both quantum and classical (FF)

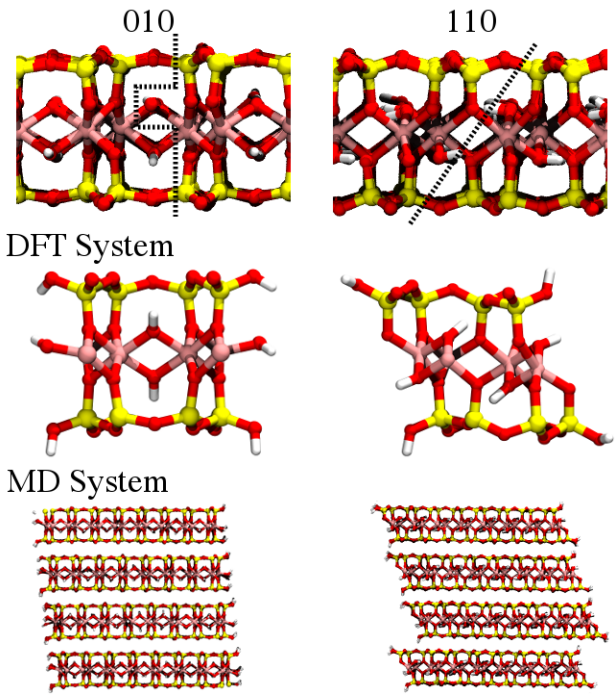

Fig 1. Three-dimensional structure of the 010 (left) and 110 (right) crystallographic faces of pyrophyllite. The point at which the clay edge is created is depicted along with the system sizes for the DFT and MD calculations.

levels of theory, in which IR frequencies of edge species can be positively identified.

One of the most widely used force fields for MD simulations of phyllosilicates is ClayFF.[14] Atomic polarizability is not included in ClayFF, but methods including polarizability in simulations of bulk phyllosilicates have recently been developed.[15] Recent studies have shown the deficiencies in ClayFF for phyllosilicate edges which has made these simulations intractable.[5a, 16] However, Pouvreau et al. showed that the addition of a harmonic metal-O-H (M-O-H) angle bending term vastly improves the structure of gibbsite and brucite edges described with ClayFF.[17] Using these new parameters, classical MD simulations of two unique pyrophyllite edges were performed (Fig. 1) and the IR lineshape was calculated from the Fourier transform of the electrical flux-flux time correlation function (eq. 3, ESI†).[18] Direct comparisons are made to the quantum spectrum calculated using density functional perturbation theory and the experimental IR spectra of dry deuterated samples (see ESI† for full computational/experimental methods).

The experimental IR spectrum for the as-received (non-deuterated) pyrophyllite sample is shown in Fig. 2. Edges will, of course, exist however the signal from the edge groups will be dominated by internal Al-O-H groups, so the experimental spectrum is compared with MD simulations of bulk pyrophyllite. The spectra obtained from MD were calculated from simulations with and without the recently derived M-O-H (M = Si or Al) angle bending terms in ClayFF.[17] The experimental spectrum shows the Al-O-H stretch appearing at ~3675 cm^{-1}, consistent with previous experimental studies.[19] Interestingly, the angle bending term causes the simulated Al-O-H stretch to shift from 3690 cm^{-1} to 3640 cm^{-1}.

However, using the angle bending term results in a clear improvement in the bending region of the calculated spectra. Experimentally, broad peaks are observed at 1125 cm^{-1}, 1060 cm^{-1}, 1040 cm^{-1}, and 940 cm^{-1}. Without the angle bending term, only two peaks are seen in the bending region of the simulated spectrum, with minimal overlap with the experimental spectrum. Inclusion of the angle bending term greatly increases the agreement with experiment, particularly with the 1040 cm^{-1} peak. Moreover, a previously absent, third peak is observed at 970 cm^{-1}; albeit with less agreement with the experimental peak at 940 cm^{-1}.

With clear evidence in hand that the angle bending terms increase the accuracy of the structure of bulk pyrophyllite, we next turn our attention towards edge structures after deuteration. Classical MD results for the deuterated 010 and 110 faces along with the experimental spectrum are shown in Fig. 3. A broad experimental band is observed at 2485 cm^{-1}

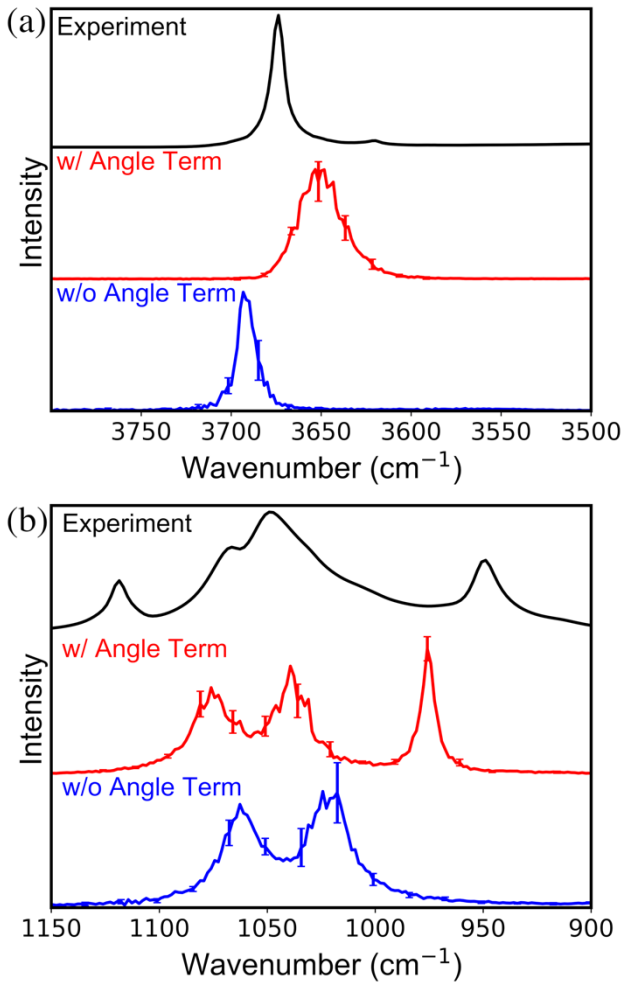

Fig 2. Infrared spectrum of bulk protonated pyrophyllite calculated from classical MD simulation with the angle bending term (red) and without (blue), with direct comparisons to experimental results (black). Results are shown for the (a) stretching and (b) bending regions.

which is likely bulk D_2O. Peaks at 2362 cm^{-1} and 2341 cm^{-1} are due to atmospheric CO_2. A small peak, seen at 2721 cm^{-1}, persists after drying (Fig. S7, ESI† for successive drying spectra), which we attribute to an edge O-D stretch. This is in excellent agreement with the MD results, where O-D stretching modes at edge silanol and aluminol groups occur in the 2550-2750 cm^{-1} range. The experimental spectrum is not sufficiently resolved to determine if the O-D stretching mode at 2721 cm^{-1} is due to silanol or aluminol groups, or both. Additional experiments on another layered mineral such as gibbsite or kaolinite would help to identify the frequency of an edge (Al)O-D stretch, but the presence of aluminol groups on the basal surfaces of these minerals would likely interfere with peak identification. However, it appears probable that the 2721 cm^{-1} peak is due to deuteration on the 010 face as more overlap exists between the simulated 010 spectrum and this experimental peak. Moreover, we speculate that this peak (2721 cm^{-1}) is due to groups forming hydrogen bonds. Hydrogen bonding, in addition to red shifting the O-H stretch frequency, increases the adsorption intensity.[20] Given that only a single peak exists above the broader D_2O band, it stands to reason that only the most intense peak would appear (i.e. hydrogen bound groups). We note that a more hydrophilic phyllosilicate (e.g., montmorillonite) would likely be more susceptible to deuterium exchange at the edge and might generate a better signal to noise ratio in this spectral region.

Distinct changes in the bending region for deuterated samples are observed in both the experimental and calculated spectra (Fig. S8, ESI†). In particular, the experimental peak observed in protonated pyrophyllite at 1060 cm^{-1} (Fig. 2b) becomes broader and a new small peak is observed at 890 cm^{-1}. We note in the calculated spectra that the peak originally observed at 1040 cm^{-1} is blue shifted on the 110 face. The experimental spectrum is possibly capturing an ensemble average of several crystallographic faces leading to the experimentally observed broadening affect. Moreover, a new peak at 890 cm^{-1} is observed in the calculated 010 spectrum which closely aligns with the weak new peak observed experimentally.

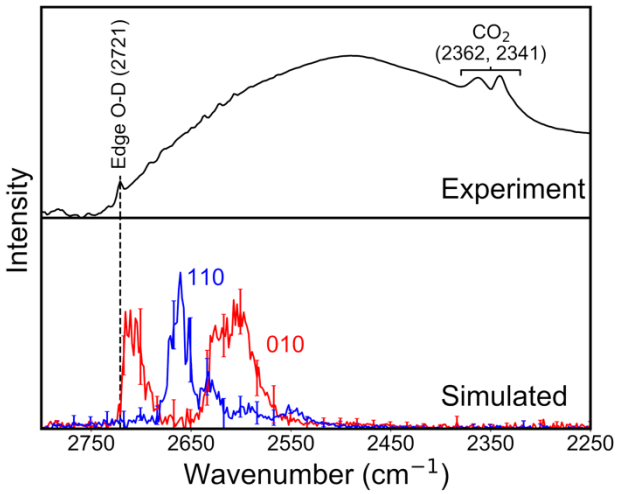

Fig 3. Experimental (top) and calculated (bottom) deuterated IR spectra for pyrophyllite in the O-D stretch region. The experimental sample was exposed to D_2O and then dried under N_2. Results for the calculated 010 (red) and 110 (blue) faces are shown. The experimental peak at 2721 cm^{-1} closely aligns with the Si-O-D and Al-O-D peaks from the simulated spectra.

The simulated spectra allow for the development of a molecular-level picture and we now discuss those results in greater detail. The full IR spectra calculated from classical MD simulations of the protonated and deuterated 010 face are shown in Fig. 4 (Fig. S9, ESI† for the 110 face). In this context DFT-calculated normal modes were used to help assign peaks from the classical simulations (Fig. S10 and S11, ESI† for the DFT spectra of the 010 and 110 faces). This is particularly instructive in the stretching region and we discuss these results first. On the 010 edge, Si-O-H normal modes appear around 3730 cm^{-1} for non-hydrogen bound groups, and 3525/3480 cm^{-1} for hydrogen bound groups. While on the 110 edge, Si-O-H stretches are observed at 3800 cm^{-1} and 3250 cm^{-1} for non-hydrogen bound and hydrogen bound groups respectively. Layer-layer hydrogen bonding is responsible for the nearly 200 cm^{-1} and 600 cm^{-1} red shift in the stretching modes. We note that interlayer hydrogen bonding on the 110 face is significantly stronger than the 010 face. This is due, in part, to the cleavage

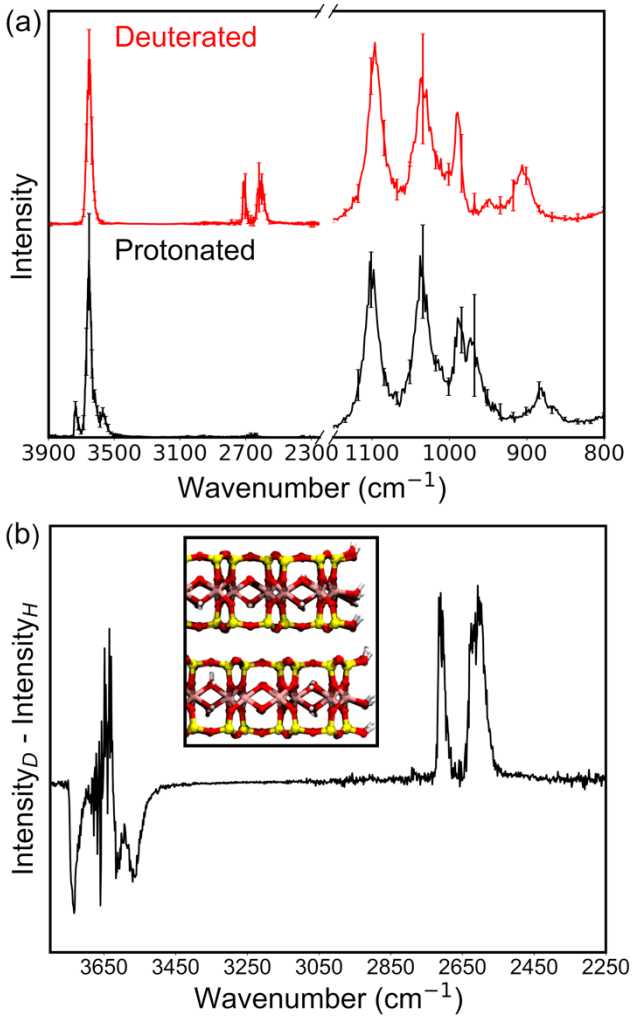

Fig 4. (a) Full infrared spectrum of the protonated (black) and deuterated (red) 010 pyrophyllite edge and (b) difference spectrum between deuterated and protonated spectra for the stretching region. In this spectrum negative peaks represent those that were shifted due to deuteration and positive peaks represent their new positions.

angle in the cut which results in hydrogen bonding occurring between edge hydroxyls and basal plane siloxanes (Fig. 1). Edge Al-O-H stretches are seen around 3800 cm^{-1} for both faces. Deuteration of all edge hydroxyl groups results in a red shift of approximately 1000 cm^{-1}. While specific peak assignments can be made from the DFT spectra, qualitatively similar features are observed in the classical MD results. In this case, the internal Al-O-H groups dominate much of the spectrum, specifically within the protonated region (above 3400 cm^{-1}). Therefore, a more useful way to view the results is via a difference spectrum (i.e., subtracting the protonated spectrum from the deuterated spectrum). In this type of spectrum negative peaks in the stretching region will indicate modes that shifted upon deuteration. This result for the 010 surface is depicted in Fig. 4b (Fig. S9, ESI† for the 110 face). We observe negative peaks at 3700 cm^{-1}, 3600 cm^{-1}, and 3550 cm^{-1}. The observation of three edge peaks is consistent with the normal mode analysis and therefore we assign the peak at 3700 cm^{-1} to edge AlOH and non-H-bonded SiOH groups, and the peaks at 3550 cm^{-1} and 3600 cm^{-1} to two different populations of H-bonded SiOH groups. The 110 face has much broader features, however we observe negative peaks at 3700 cm^{-1}, 3650 cm^{-1}, and a broad peak at 3550 cm^{-1}. We attribute these broader features to the 110 face forming hydrogen bonds between edge SiOHs and siloxane oxygens (Fig. 1). The broader range of hydrogen bonding environments in the 110 face leads to broader features in the IR spectrum.

In summary, using deuterium exchange, IR modes due to hydroxyl groups at edge sites of a neutral layered phyllosilicate (pyrophyllite) were isolated from modes due to layer hydroxyl groups at internal sites. This proof of concept study was performed on the most hydrophobic member of the phyllosilicate family. Despite this, a sufficient signal to noise ratio was obtained to positively identify edge vibrations. Similar approaches would likely be more effective on hydrophilic phyllosilicates (e.g., montmorillonite). The experimental results were confirmed by comparison with spectra computed from MD simulation on idealized edge models of pyrophyllite. Near quantitative agreement was observed between the experimental and classically simulated spectra. To the best of our knowledge this is the first direct observation of the IR modes associated with clay edges with direct comparisons between computational and experimental results. Additionally, validation with DFT demonstrates that the modified ClayFF force field is viable for clay edge simulations and should continue to be used with confidence.

This work was supported by the US Department of Energy, Office of Science, Office of Basic Energy Sciences, Chemical Sciences, Geosciences and Biosciences Division. Sandia National Laboratories is a multimission laboratory managed and operated by National Technology and Engineering Solutions of Sandia, LLC., a wholly owned subsidiary of Honeywell International, Inc., for the U.S. Department of Energy's National Nuclear Security Administration under contract DE-NA-0003525. The views expressed in this article do not necessarily represent the views of the U.S. Department of Energy or the United States Government.

Conflicts of interest

There are no conflicts to declare

Notes and references

1. G. Sposito, *The Surface Chemistry of Soils*, Oxford University Press, New York, 1984.
2. F. Bergaya and G. Lagaly, *Handbook of Clay Science*, London: Elsevier, London, 2013.
3. (a) X. Liu, X. Lu, R. Wang and H. Zhou, *Geochim. Cosmochim. Acta*, 2008, **72**, 1837-1847; (b) S. L. Teich-McGoldrick, J. A. Greathouse, C. F. Jové-Colón and R. T. Cygan, *J. Phys. Chem. C*, 2015, **119**, 20880-20891; (c) M. Rahromostaqim and M. Sahimi, *J. Phys. Chem. C*, 2018, **122**, 14631-14639.
4. L. Dzene, E. Tertre, F. Hubert and E. Ferrage, *J. Colloid Interface Sci.*, 2015, **455**, 254-260.
5. (a) K. Yu and J. R. Schmidt, *J. Phys. Chem. C*, 2011, **115**, 1887-1898; (b) T. Underwood, V. Erastova, P. Cubillas and H. C. Greenwell, *J. Phys. Chem. C*, 2015, **119**, 7282-7294; (c) M. Sedghi, M. Piri and L. Goual, *Langmuir*, 2016, **32**, 3375-3384; (d) J. A. Greathouse, R. T. Cygan, J. T. Fredrich and G. R. Jerauld, *J. Phys. Chem. C*, 2017, **121**, 22773-22786.
6. (a) C. Tournassat, A. Neaman, F. Villiéras, D. Bosbach and L. Charlet, *Am. Miner.*, 2003, **88**, 1989-1995; (b) M. Sayed Hassan, F. Villieras, F. Gaboriaud and A. Razafitianamaharavo, *J. Colloid Interface Sci.*, 2006, **296**, 614-623.
7. C. J. Chisholm-Brause, J. M. Berg, R. A. Matzner and D. E. Morris, *J. Colloid Interface Sci.*, 2001, **233**, 38-49.
8. M. Rashad, E. Elnaggar and F. F. Assaad, *Environ. Earth Sci.*, 2013, **71**, 3855-3864.
9. R. M. Tinnacher, M. Holmboe, C. Tournassat, I. C. Bourg and J. A. Davis, *Geochim. Cosmochim. Acta*, 2016, **177**, 130-149.
10. (a) R. L. Parfitt, J. D. Russell and V. C. Farmer, *J. Chem. Soc., Faraday Trans. 1*, 1976, **72**; (b) C. H. Rochester and S. A. Topham, *J. Chem. Soc., Faraday Trans. 1*, 1979, **75**; (c) X. Sun and H. E. Doner, *Soil Science*, 1996, **161**, 865-872.
11. (a) V. C. Farmer and J. D. Russell, *Trans. Faraday Soc.*, 1971, **67**, 2737-2749; (b) A. Kuligiewicz, A. Derkowski, M. Szczerba, V. Gionis and G. D. Chryssikos, *Clays and Clay Miner.*, 2015, **63**, 15-29; (c) A. Kuligiewicz, A. Derkowski, J. Środoń, V. Gionis and G. D. Chryssikos, *Appl. Clay Sci.*, 2018, **161**, 354-363; (d) C. Tsiantos, V. Gionis and G. D. Chryssikos, *Appl. Clay Sci.*, 2018, **160**, 81-87.
12. (a) R. F. Giese, P. M. Costanzo and C. J. van Oss, *Phys. Chem. Miner.*, 1991, **17**, 611-616; (b) X. Ou, Z. Lin and J. Li, *Chem. Commun.*, 2018, **54**, 5418-5421.
13. B. Rotenberg, A. J. Patel and D. Chandler, *J. Am. Chem. Soc.*, 2011, **133**, 20521-20527.
14. R. T. Cygan, J.-J. Liang and A. G. Kalinichev, *J. Phys. Chem. B*, 2004, **108**, 1255-1266.
15. (a) S. Tesson, M. Salanne, B. Rotenberg, S. Tazi and V. Marry, *J. Phys. Chem. C*, 2016, **120**, 3749-3758; (b) S. Tesson, W. Louisfrema, M. Salanne, A. Boutin, B. Rotenberg and V. Marry, *J. Phys. Chem. C*, 2017, **121**, 9833-9846.
16. (a) D. M. S. Martins, M. Molinari, M. A. Gonçalves, J. P. Mirão and S. C. Parker, *J. Phys. Chem. C*, 2014, **118**, 27308-27317; (b) A. G. Newton and G. Sposito, *Clays and Clay Miner.*, 2015, **63**, 277-289.
17. M. Pouvreau, J. A. Greathouse, R. T. Cygan and A. G. Kalinichev, *J. Phys. Chem. C*, 2017, **121**, 14757-14771.
18. P. Bornhauser and D. Bougeard, *J. Phys. Chem. B*, 2001, **105**, 36-41.
19. V. C. R. Farmer, J.D., *Spectrochim. Acta*, 1964.
20. B. Athokpam, S. G. Ramesh and R. H. McKenzie, *Chem. Phys.*, 2017, **488-489**, 43-54.

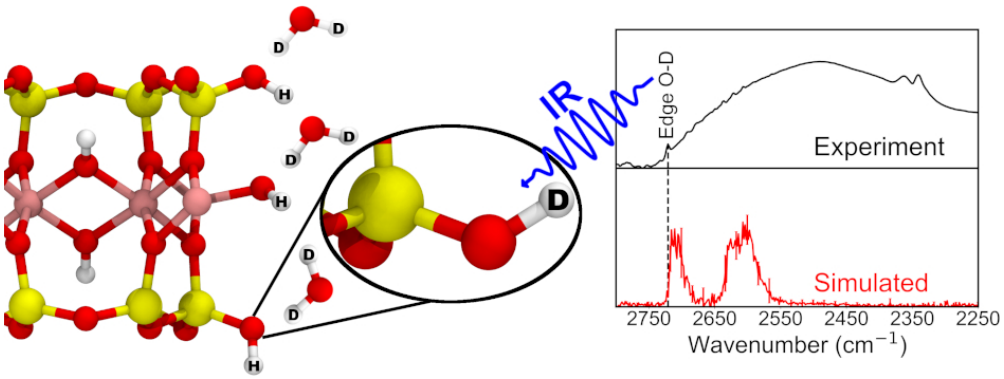

80x30mm (300 x 300 DPI)